Supplemental Information

Neuronal firing patterns outweigh circuitry oscillations in parkinsonian motor control

Ming-Kai Pan,[1,2] Sheng-Han Kuo,[3] Chun-Hwei Tai,[2] Jyun-You Liou,[4] Ju-Chun Pei,[5] Chia-Yuan Chang,[5] Yi-Mei Wang,[6] Wen-Chuan Liu,[2] Tien-Rei Wang,[2] Wen-Sung Lai[5,7] and Chung-Chin Kuo[2,7,8*]

[1]Department of Medical Research, National Taiwan University Hospital, Taipei, Taiwan

[2]Department of Neurology, National Taiwan University Hospital, Taipei, Taiwan

[3]Department of Neurology, College of Physicians and Surgeons, Columbia University, New York, NY, USA

[4]Department of Physiology and Cellular Biophysics, Columbia University, New York, NY, USA

[5]Department of Psychology, National Taiwan University, Taipei, Taiwan

[6]Department of Neurology, National Taiwan University Hospital, Yun-Lin Branch, Yun-Lin, Taiwan

[7]Neurobiology & Cognitive Science Center, National Taiwan University, Taipei, Taiwan

[8]Department of Physiology, National Taiwan University, Taipei, Taiwan

*Corresponding author. Email: chungchinkuo@ntu.edu.tw

This PDF file includes:

Supplemental Figures 1 to 13

Legends for Supplemental Videos 1 to 4

Full Methods
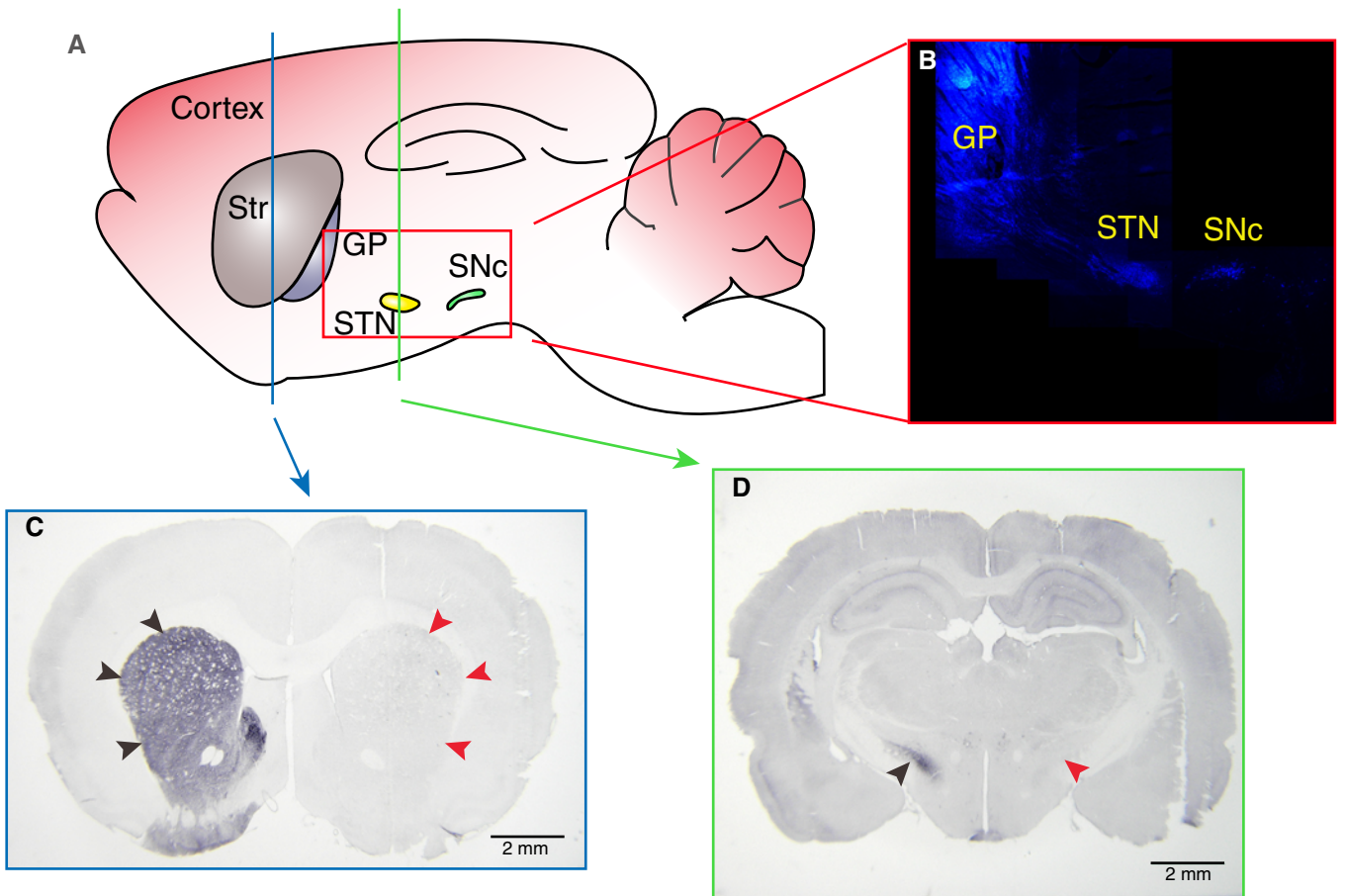
Supplemental Figure 1. Histological verification of 6-OHDA lesioned hemiparkinsonian rats. (**A**) Schematic locations of main deep brain nuclei in the basal ganglia circuitry. (**B**) Retrograde tracing of deep brain structures by injecting fluorogold into STN. Globus pallidus (GP) and substantia nigra pars compacta (SNc) are two nuclei directly innervating STN. (**C** and **D**) Images of tyrosine hydroxylase immunohistochemistry in an unilateral 6-OHDA lesioned rat. The (C) striatum and (D) STN developed unilateral loss of dopaminergic innervation ipsilateral to the lesioned side (red arrow heads).
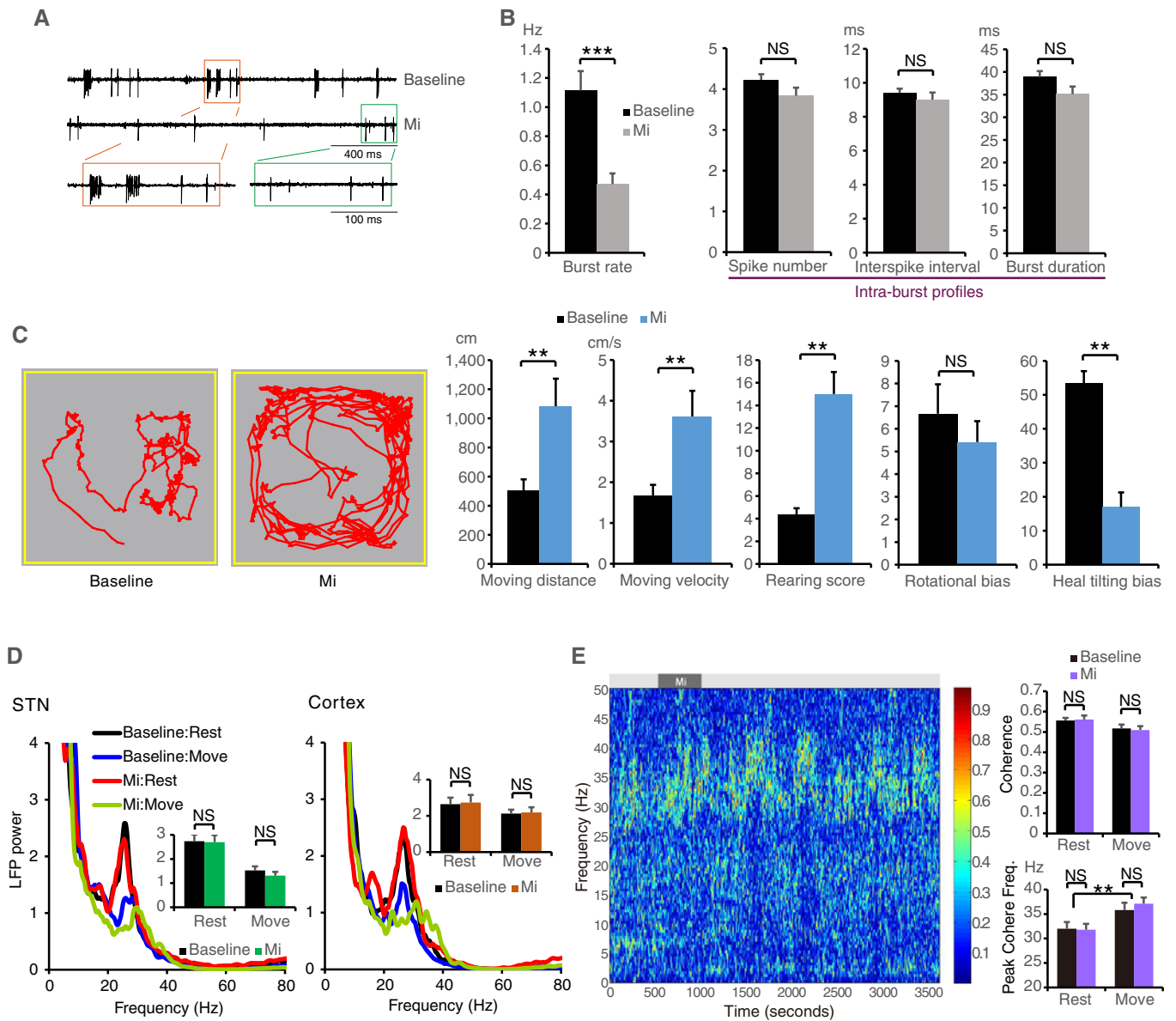
Supplemental Figure 2. Behavioral and electrophysiological changes by subthalamic infusion of mibefradil in 6-OHDA rats. (**A** and **B**) Sample sweeps and quantitative analysis of single-unit firings. Mibefradil (Mi), a CaT blocker, suppressed burst firings without changing the intra-burst profiles in 6-OHDA rats ($n = 42$). (**C-E**) Mibefradil microinfusion rescued (C) locomotor behaviors ($n = 12$), but had no effect on either (D) in-situ synchronization in cortex and STN, or (E) cortico-subthalamic oscillations ($n = 11$). Data are presented as mean ± s.e.m., **$P < 0.01$, ***$P < 0.001$, NS: not significant.
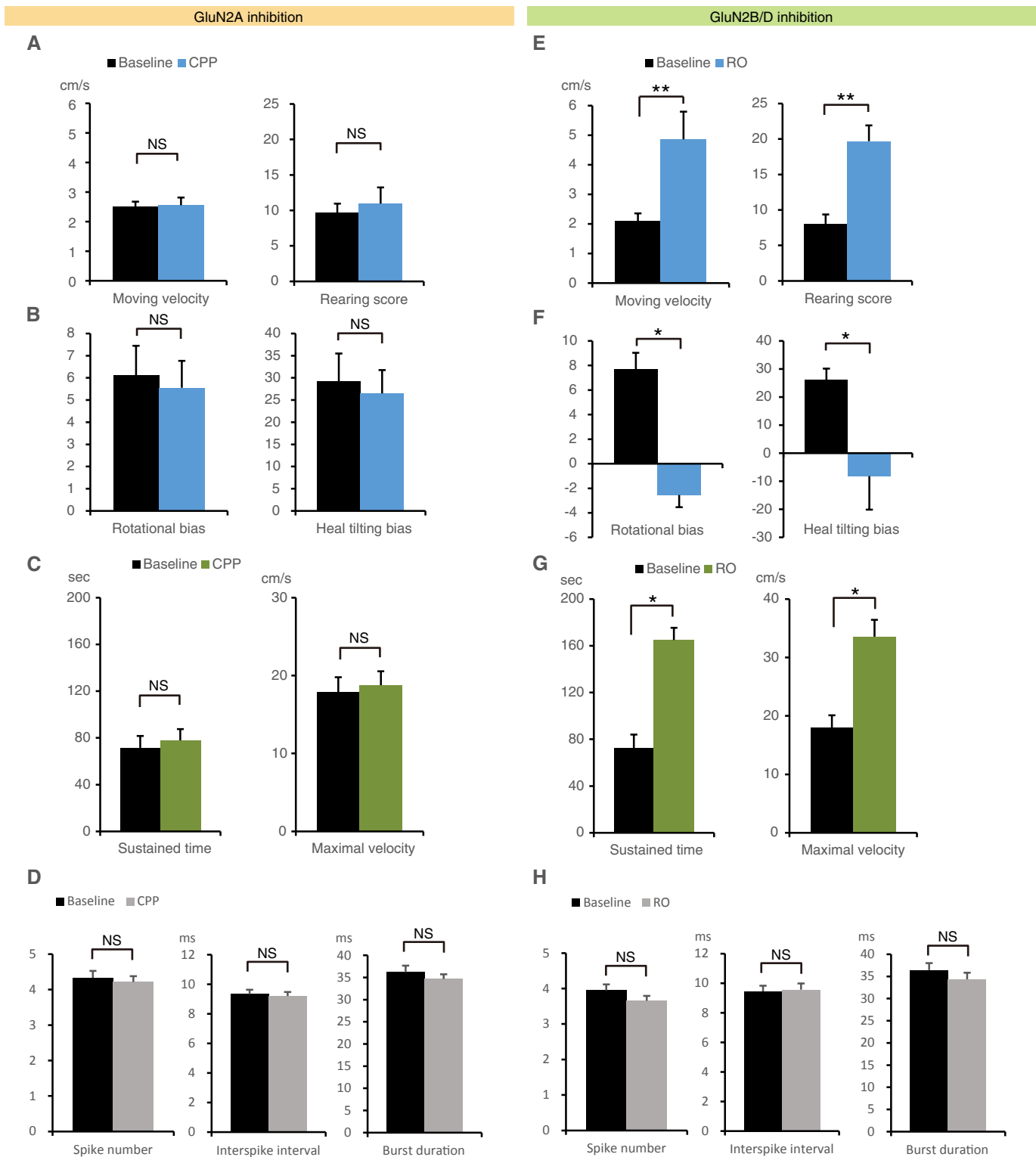
Supplemental Figure 3. Auxiliary behavioral and single-unit profiles of 6-OHDA rats receiving subthalamic infusion of CPP or RO in 6-OHDA rats. (**A-C**) CPP did not change (A) animal motilities or (B) asymmetric movements in free-moving paradigm (*n* = 18). It also failed to improve (C) forced-moving behaviors (*n* = 9). (**D**) CPP had no effect on intra-burst profiles, including spike number in each burst, inter-spike interval between each spike in burst, and burst duration (*n* = 29). (**E-G**) RO ameliorated motility deficits and motion asymmetries in free-moving paradigms (*n* = 13), as well as forced-moving behaviors (*n* = 7). (**H**) RO suppressed burst firings (Figure 4F) but had no effect on intra-burst profiles (*n* = 38). Data are presented as mean ± s.e.m., *$P < 0.05$, **$P < 0.01$, NS: not significant.
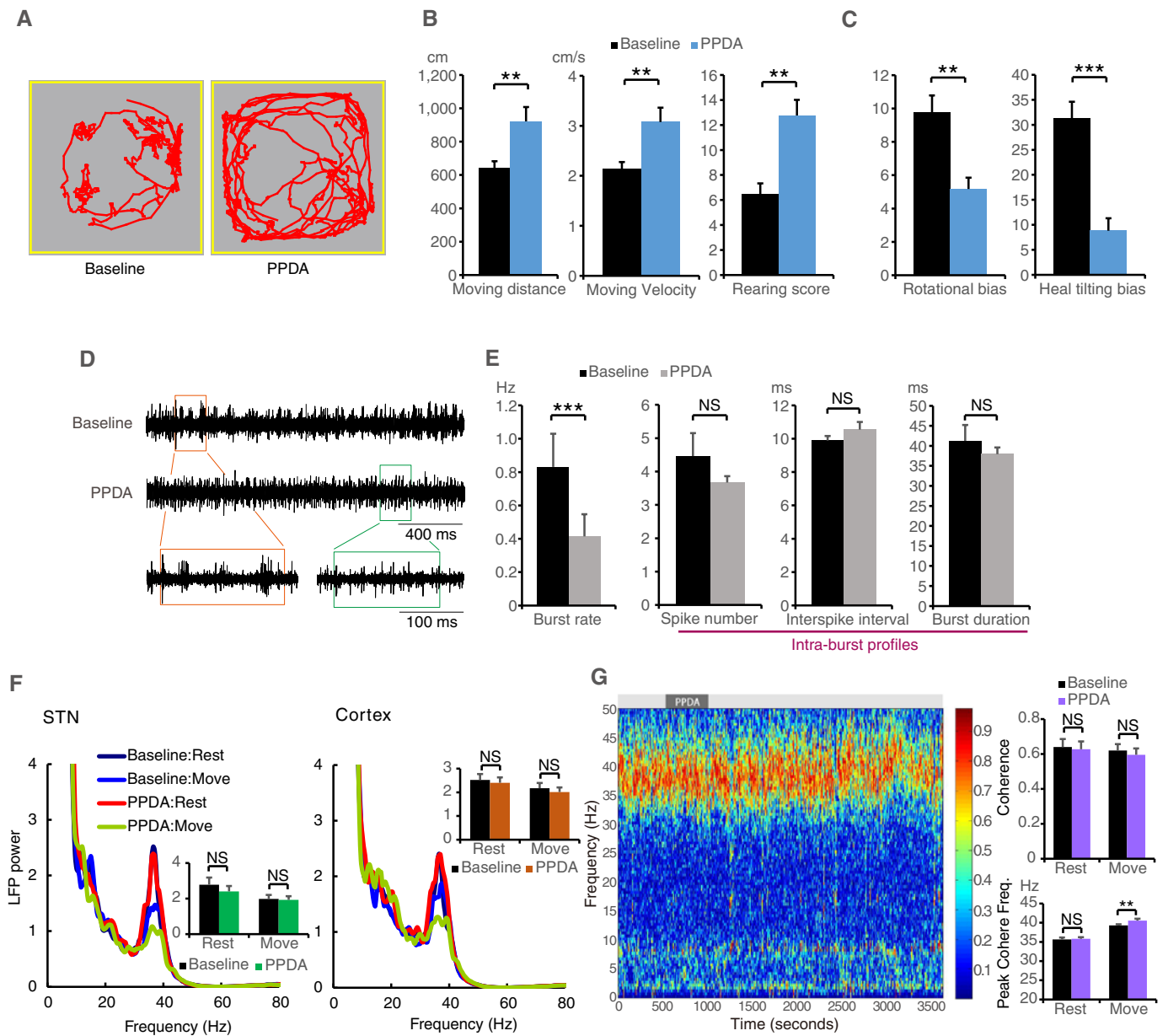
Supplemental Figure 4. Behavioral and electrophysiological changes by subthalamic infusion of PPDA in 6-OHDA rats. PPDA is a selective GluN2B/D blocker preferentially inhibiting GluN2D subunit. (**A-C**) Sample traces and quantitative analysis of locomotor behaviors. PPDA ameliorated the (B) hypokinetic and (C) asymmetric movements in 6-OHDA rats (n = 17). (**D** and **E**) Single-unit firings in STN. PPDA suppressed burst firings, without changing the intra-burst profiles of each burst (n = 14). (**F** and **G**) Oscillatory profiles. PPDA did not change (f) in-situ synchronization or (g) cortico-subthalamic oscillations (n = 15). Data are presented as mean ± s.e.m., **P < 0.01, ***P < 0.001, NS: not significant.
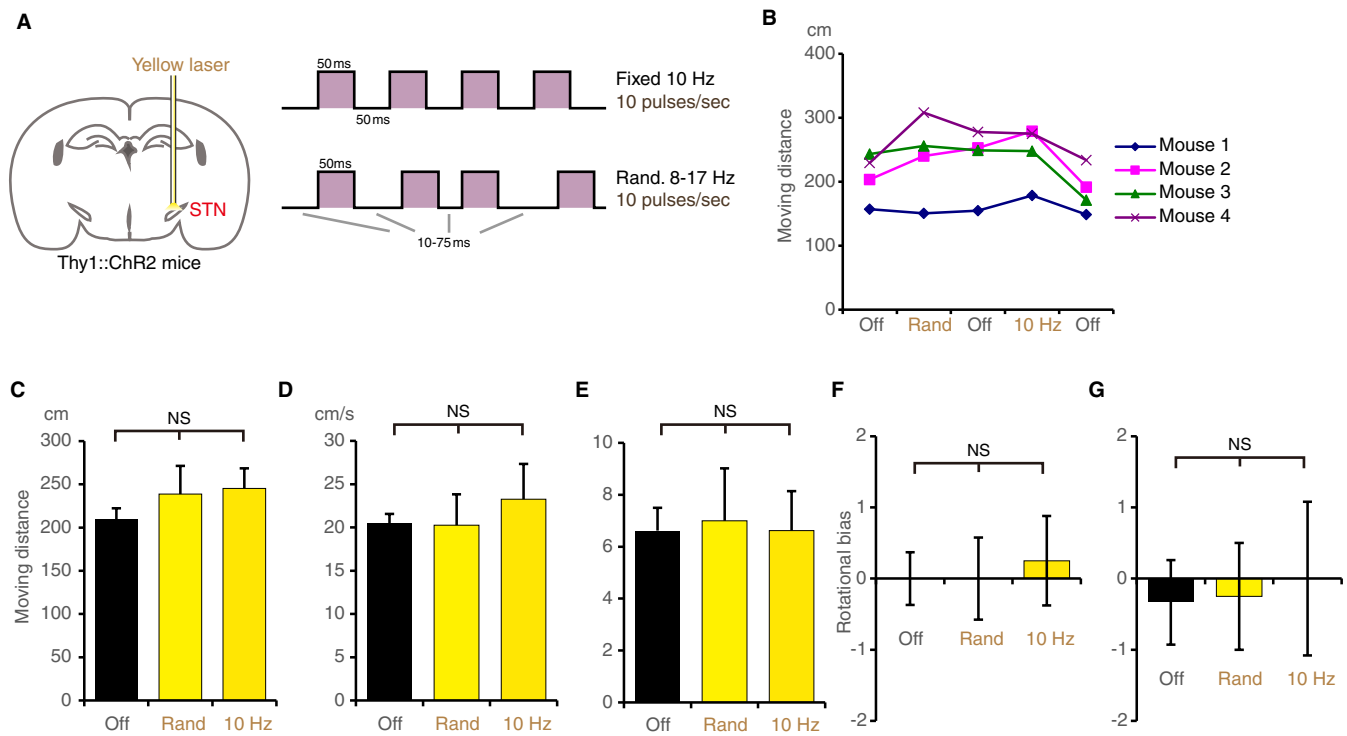
Supplemental Figure 5. Thermodynamic control of cortico-subthalamic illumination in STN. (A) The experimental protocols and readouts were the same as those in Figure 5, except the laser wavelength. Yellow laser (wavelength: 589 nm), used for controlled illumination, provided the same thermal energy (4 mW) as blue laser (473 nm) without opening channelrhodopsin-2. **(B-G)** In contrast to blue light, which induced bradykinesia in both randomized and 10-Hz protocols (Figure 5), yellow light had no behavioral effects ($n = 4$, $P > 0.6$ in all cases). Data are presented as mean ± s.e.m., NS: not significant.
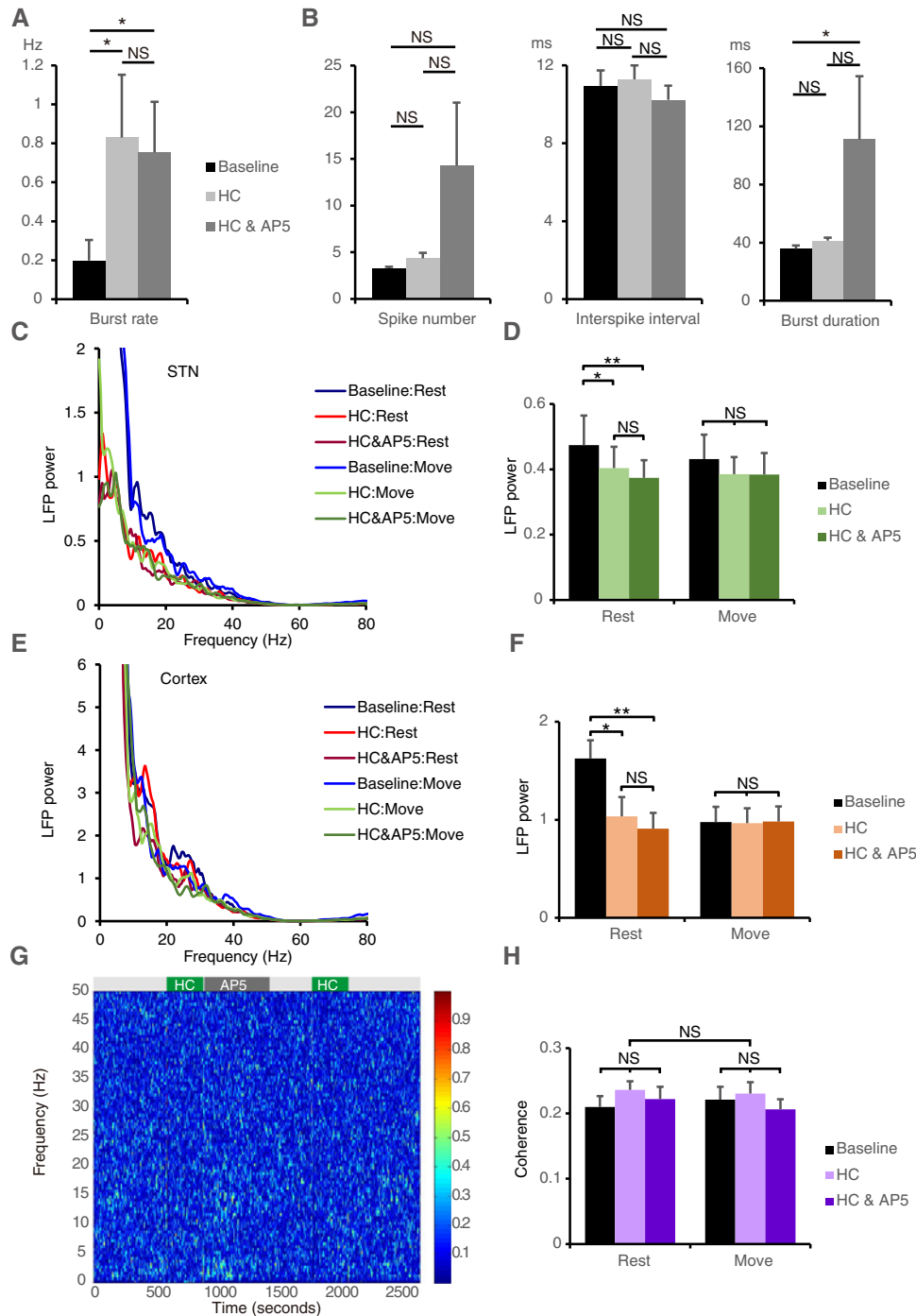
Supplemental Figure 6. Electrophysiological changes by subthalamic application of NMDAR blocker and HC in normal rats. (**A**) Quantitative burst analysis by subthalamic application of HC (200 μA), with or without simultaneous AP5 (1 mM). Additional blockage of NMDAergic cortico-subthalamic transmission by AP5 cannot reverse the burst-generating effect of HC (*n* = 18). (**B**) Intra-burst profiles. Simultaneous application of AP5 and HC had the trend to increase the spike number per burst and burst duration. (**C** and **D**) Examples and quantitative measurement of LFPs in STN. Instead of restoring beta synchronization to mimic parkinsonian state, HC, with or without simultaneous AP5, further suppressed beta LFPs in the resting states (*n* = 9). STN LFPs in the moving state were already desynchronized and remained suppressed by the manipulations. (**E** and **F**) Examples and quantitative measurement of cortical LFPs. The HC interventions in STN induced similar changes in the cortex remotely. (**G** and **H**) Time-coherence plot of cortico-subthalamic oscillations and quantitative coherence analysis. Despite the behavioral effects (Figure 6, A-D), HC, with or without simultaneous AP5, had no effect on coherence. Data are presented as mean ± s.e.m., *$P < 0.05$, **$P < 0.01$, NS: not significant.
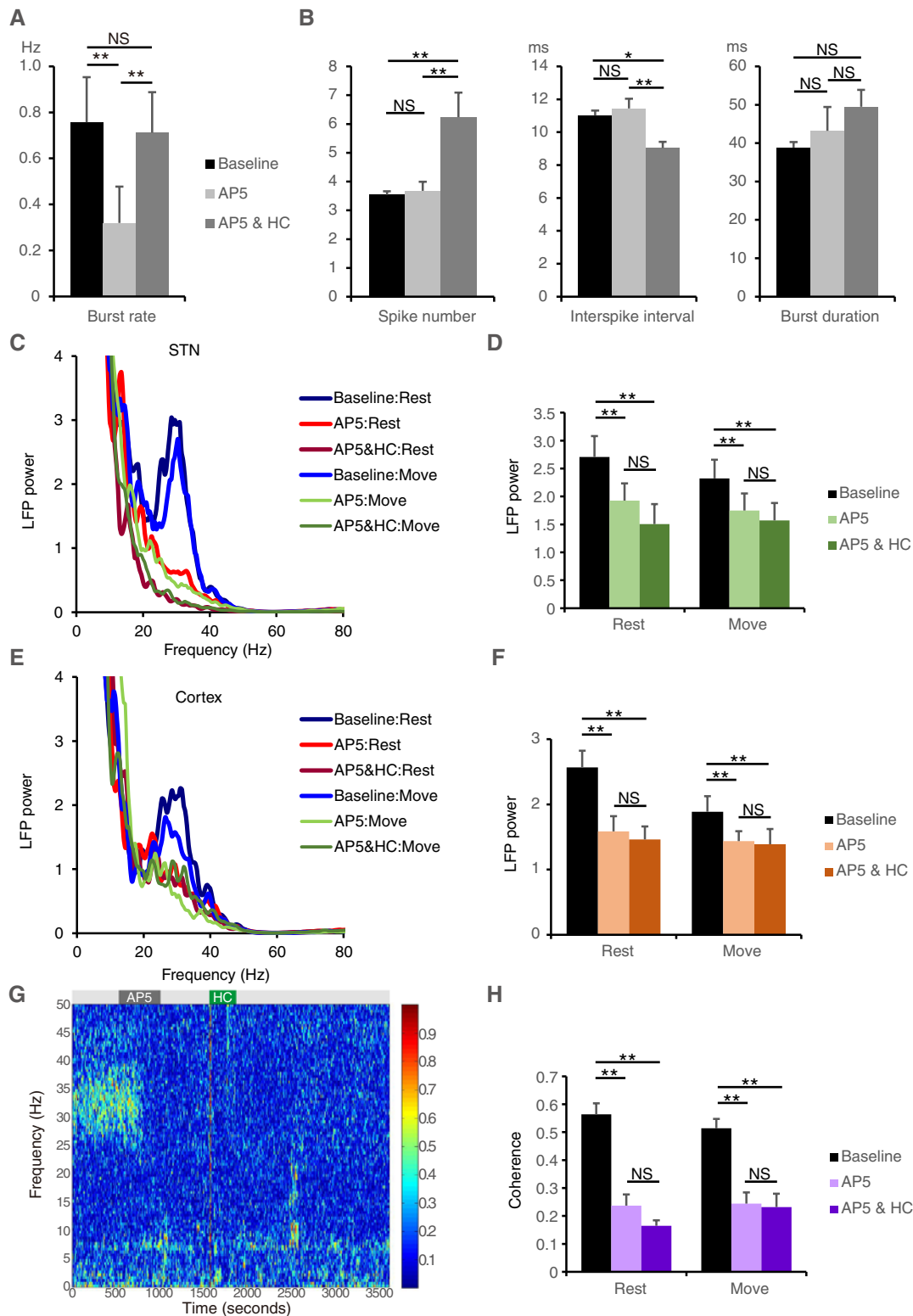
Supplemental Figure 7. Electrophysiological changes by subthalamic application of NMDAR blocker and HC in 6-OHDA rats. (**A**) Quantitative burst analysis by subthalamic application of AP5 (1 mM), with or without simultaneous HC (200 μA). The burst-suppressing effect of AP5 can be blocked by concomitant HC application (*n* = 15). (**B**) Intra-burst profiles. Simultaneous application of AP5 and HC increased the spike number per burst and shortened the inter-spike interval. (**C**-**F**) Examples and quantitative measurement of STN and cortical LFPs. AP5 significantly suppressed the beta peaks in LFPs, while simultaneous HC gave no additional change (*n* = 12). (**G**-**H**) Time-coherence plot of cortico-subthalamic oscillations and quantitative coherence analysis. AP5 suppressed beta oscillations but simultaneous HC had no additional effect. Data are presented as mean ± s.e.m., **P* < 0.05, ***P* < 0.01, NS: not significant.

7
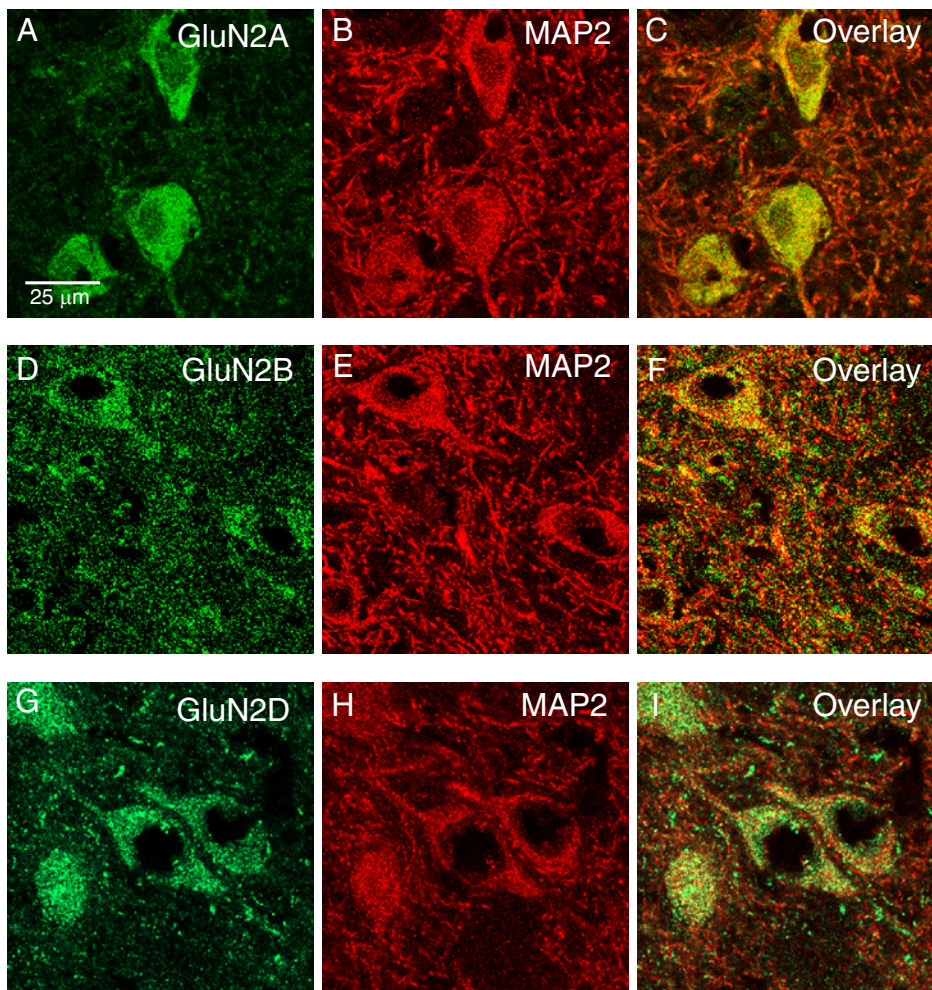
Supplemental Figure 8. Subcellular distributions of NMDAR subunits in STN of 6-OHDA rats. (A-C) Confocal images demonstrating the expression of GluN2A subunit of NMDAR and microtubule-associated protein 2 (MAP2) in STN of a 6-OHDA rat. GluN2A had a diffuse expressing pattern predominantly localized in STN cell bodies. (**D-I**) Images showing that GluN2B and GluN2D had a typical punctual pattern with additional expression in dendrites. Also refer to Supplemental Figure 13 for antigen-blocking controls.
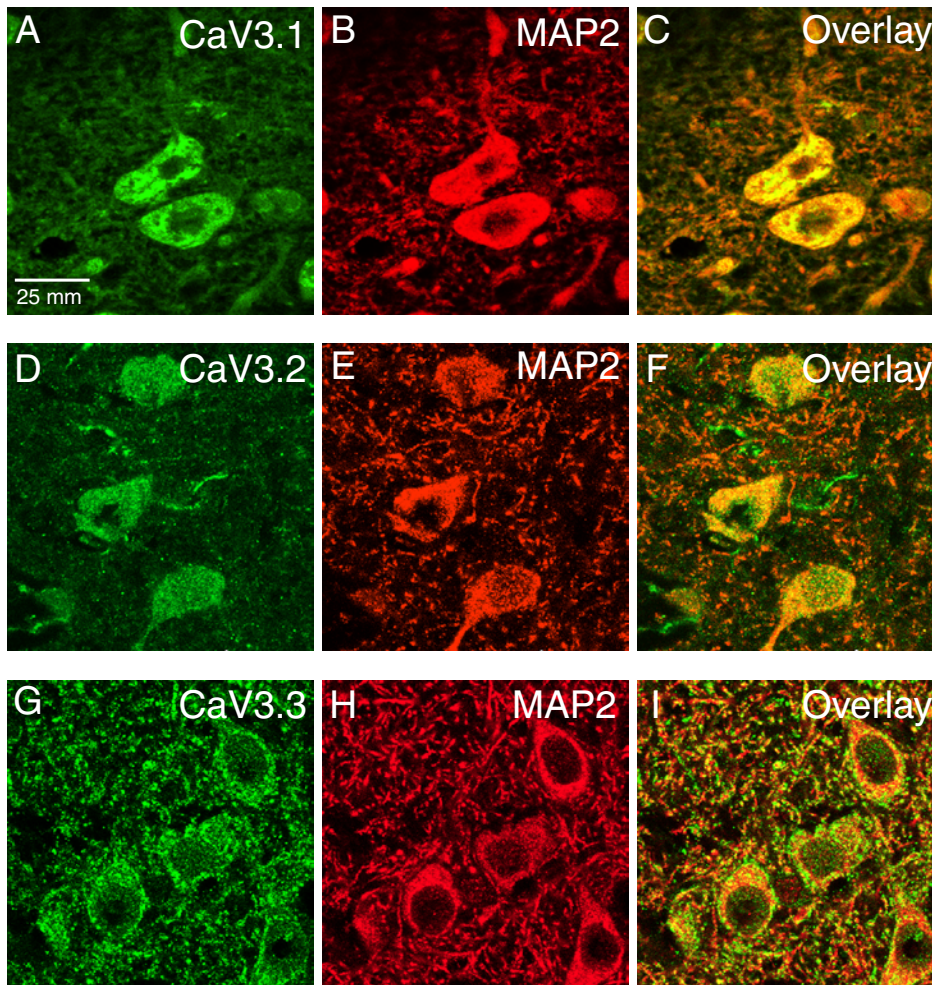
Supplemental Figure 9. Subcellular distributions of CaT subtypes in STN of 6-OHDA rats. CaTs are genetically categorized into CaV3 families and have 3 major subtypes. (**A-C**) Confocal images demonstrating the colocalization of CaV3.1 and MAP2 in STN of a 6-OHDA rat. CaV3.1 had a diffuse expression pattern mainly localized in the cell bodies. (**D-F**) Images showing that CaV3.2 had a punctual pattern with additional expression in STN dendrites. (**G-I**) Images showing that CaV3.3 also had a punctual pattern with prominent dendritic expression. Also refer to Supplemental Figure 13 for antigen-blocking controls.
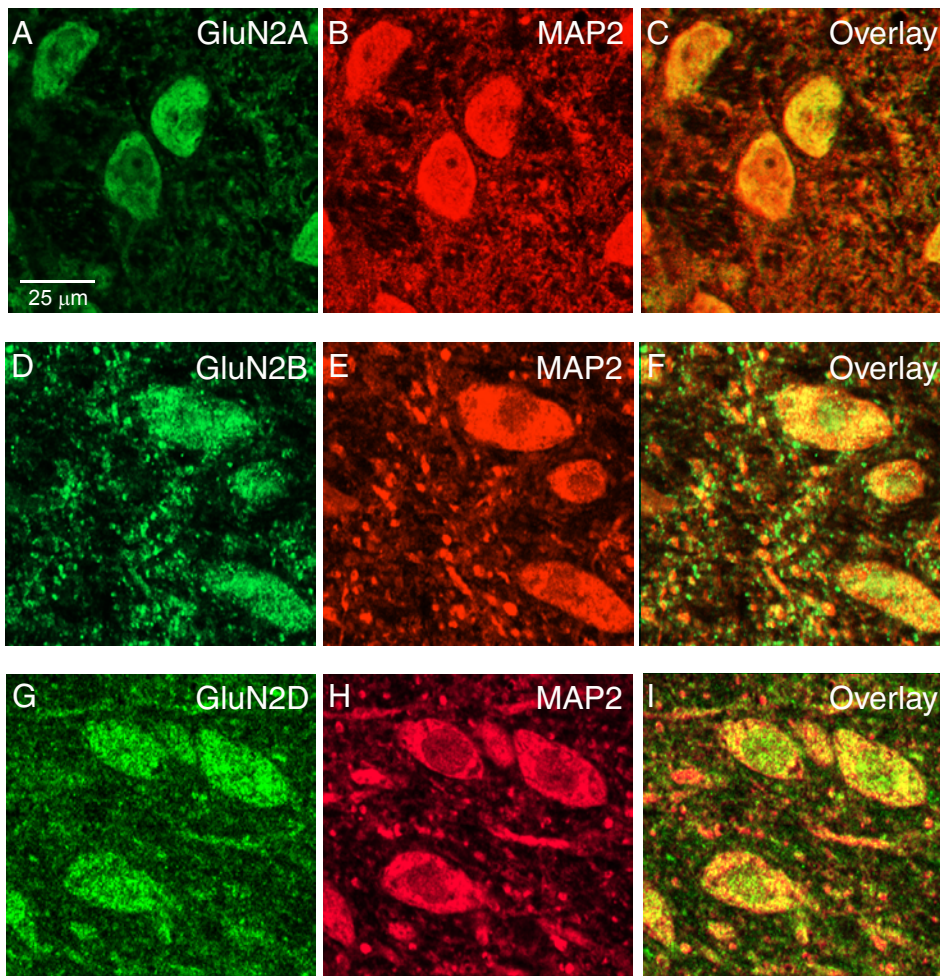
Supplemental Figure 10. Subcellular distributions of NMDAR subtypes in STN of naïve rats. (**A-C**) Confocal images demonstrating the expression of GluN2A subunit of NMDAR and MAP2 in rodent STN. GluN2A was predominantly expressed in STN cell bodies. (**D-I**) Images showing that GluN2B and GluN2D had a typical punctual pattern with additional expression in rodent STN dendrites.
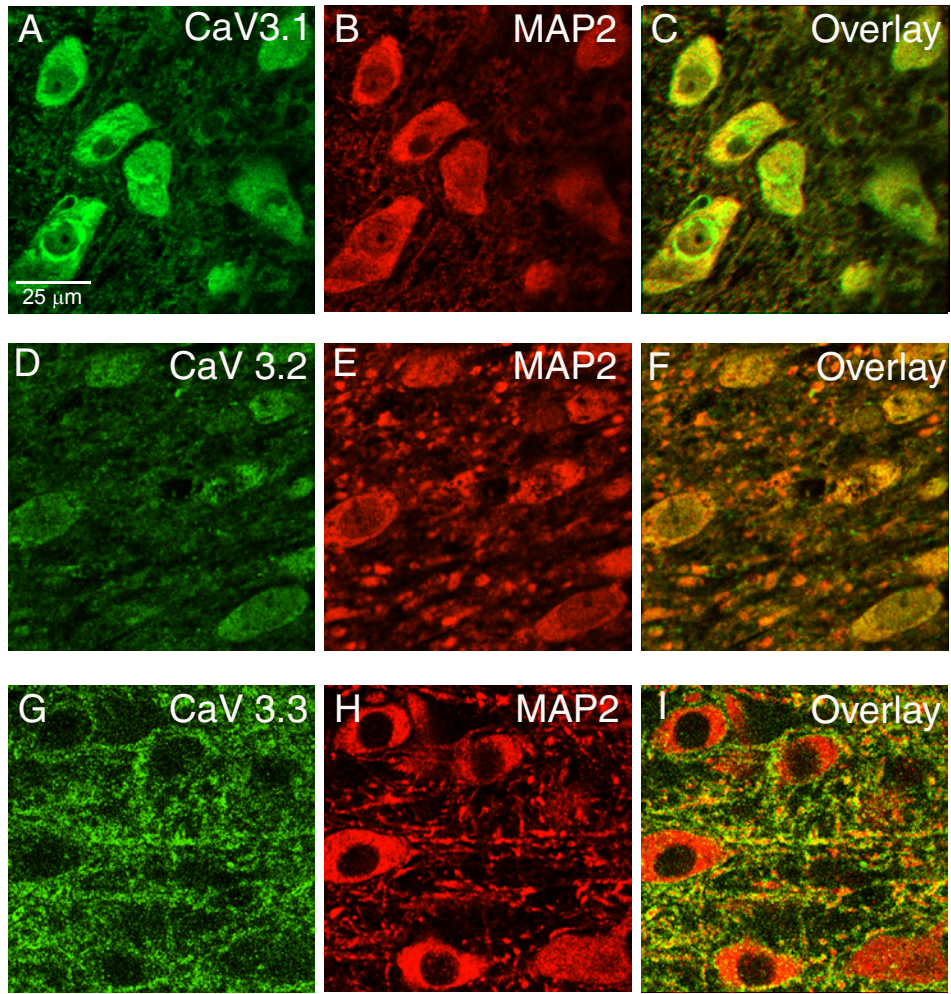
Supplemental Figure 11. Subcellular distributions of CaT subtypes in STN of naïve rats. (**A-C**) Confocal images demonstrating the colocalization of CaV3.1 and MAP2 in rodent STN. CaV3.1 had a diffuse pattern with prominent expression in the cell body. (**D-F**) Images showing that CaV3.2 was weakly expressed in rodent STN, preferentially in the cell bodies. (**G-I**) Images showing that CaV3.3 had a punctual pattern with additional expression in STN dendrites.
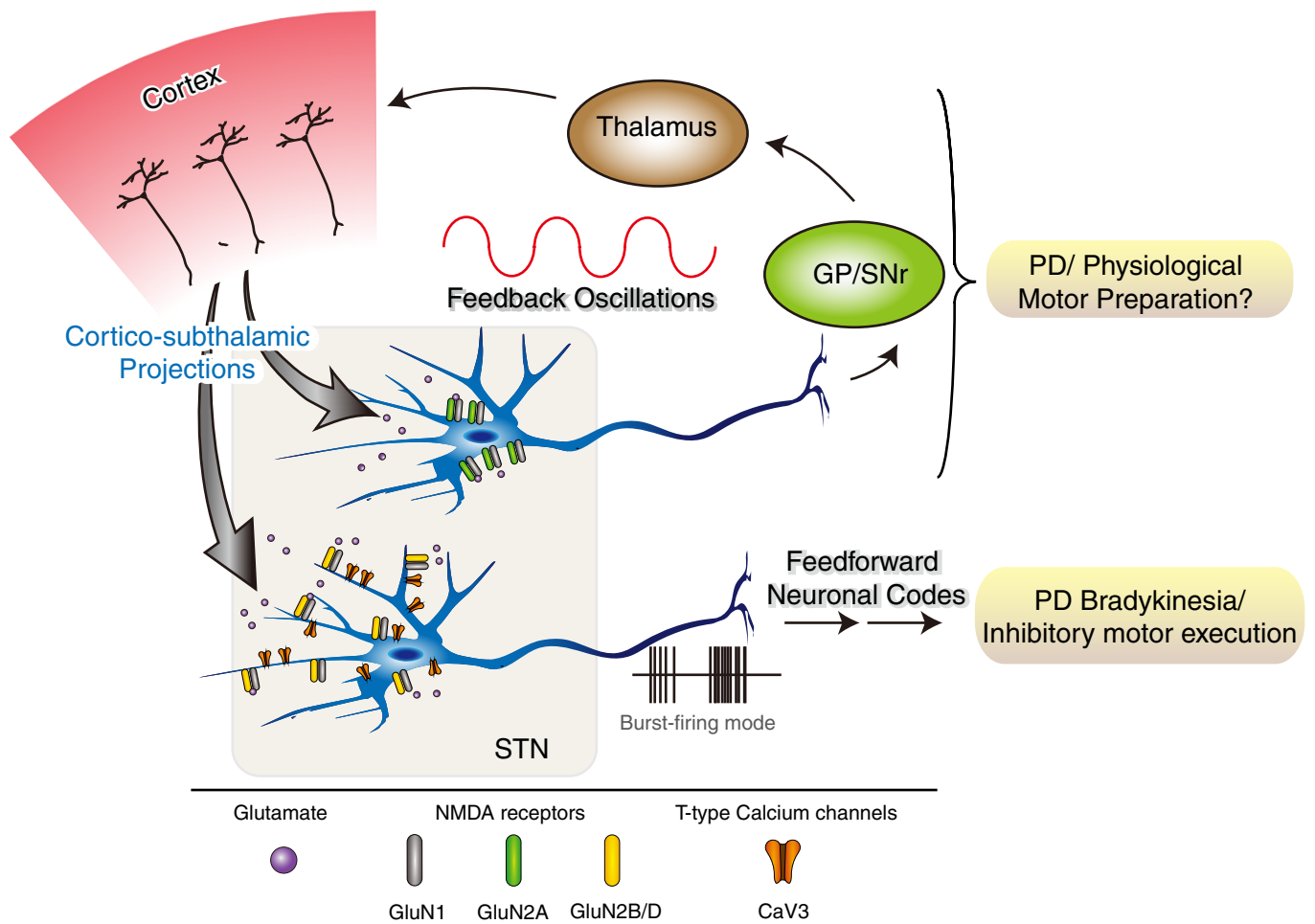
Supplemental Figure 12. Schematic summary of coding-based modifications in motor control theory.
The cortico-subthalamic regulation is an essential component of feedback neuronal oscillations, which requires GluN2A-contained NMDA receptors in STN cell body and may involve in the higher-order motor control mechanisms. The cortico-subthalamic projections also regulate bradykinesia in PD or inhibitory motor executions by feedforward neuronal codes. This mechanism requires the collaboration between GluN2B/D-contained NMDA receptors and T-type calcium channels, and facilitated by their prominent distributions in STN dendrites and cell bodies. Note that this scheme focuses on NMDA-dependent mechanism and does not include the direct and indirect pathways.
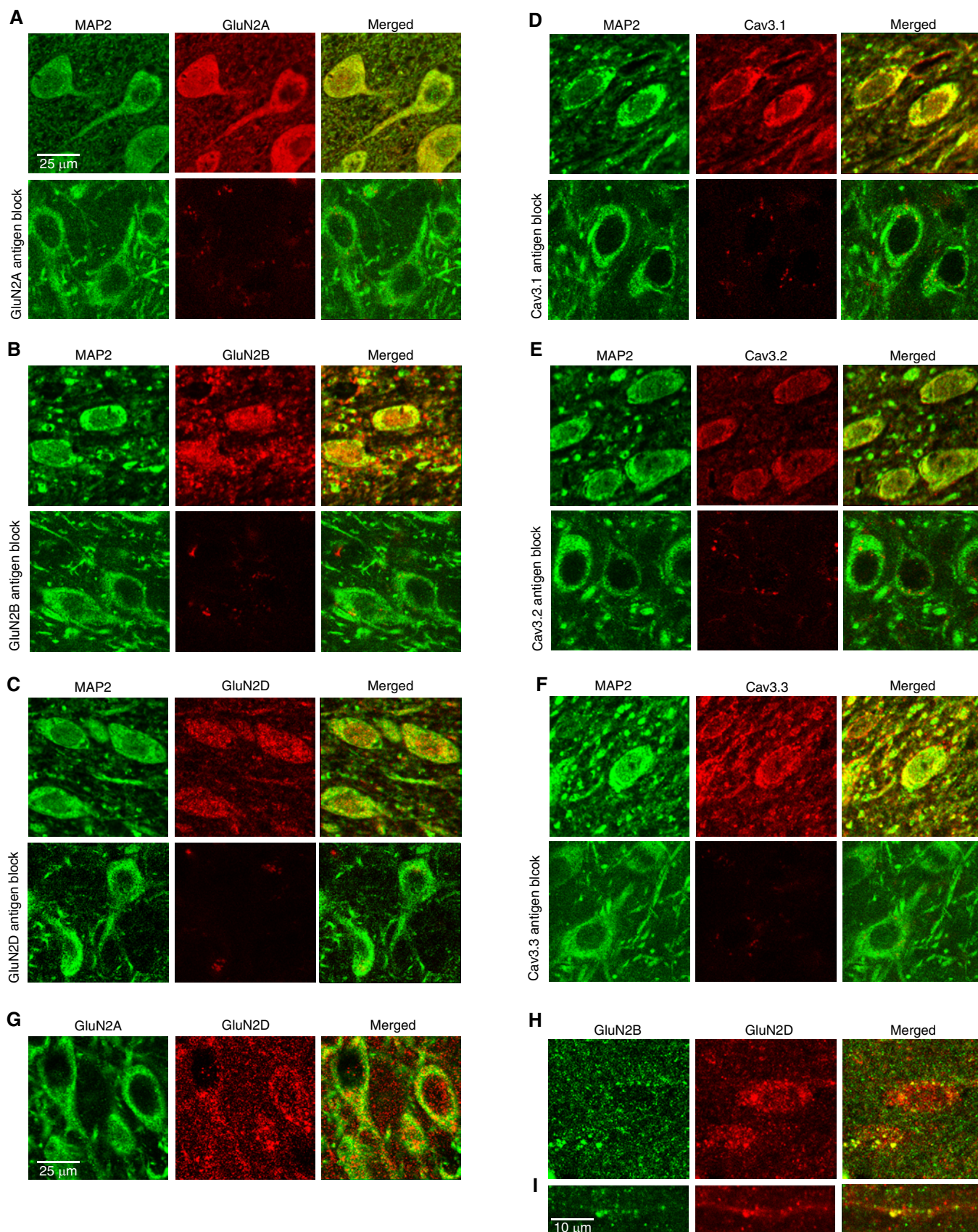
Supplemental Figure 13. Antibody specificity and colocalization of GluN2 and CaV3 antibodies in rodent STN.
(**A-F**) Confocal images demonstrating the expression of GluN2 and CaV subunits in rodent STNs. Pre-incubation of antigens with respective antibodies could effectively suppress the immunoreactivity of each receptor or ion-channel subunit. Note that figures in **C** (upper panel) are the same as Supplemental Figure 10, G-I. (**G**) GluN2A and 2D colocalization. GluN2A subunits localized predominantly in the STN soma whereas GluN2D subunits showed a punctual pattern along the STN soma and dendrites. (**H**) GluN2B and 2D colocalization. Both GluN2B and GluN2D subunits showed typical punctual patterns (upper panel) and partially colocalized in STN neurites (lower panel).

Supplemental Video 1. Free-moving behaviors in normal and 6-OHDA lesioned parkinsonian rats. This video provides head-to-head comparison between one normal rat and one 6-OHDA lesioned hemiparkinsonian rat (right-side lesioning). As compared to the normal rat, the 6-OHDA rat developed marked bradykinesia (slow movements).

Supplemental Video 2. Free-moving behaviors in 6-OHDA rats, before and after T-type calcium channel inhibition in STN. This video provides free-moving behaviors in the same 6-OHDA rat before and after $NiCl_2$ microinfusion into STN. As compared to baseline, $NiCl_2$ remedied bradykinesia in the 6-OHDA rat.

Supplemental Video 3. Free-moving behaviors in 6-OHDA rats, before and after GluN2B/D-NMDA receptor inhibition in STN. This video provides free-moving behaviors in the same 6-OHDA rat before and after RO 25-6891 (RO) microinfusion into STN. As compared to baseline, RO remedied bradykinesia in the 6-OHDA rat.

Supplemental Video 4. Unilateral illumination of cortico-subthalamic pathway in 10 Hz versus randomized protocol. We stimulated cortico-subthalamic pathway in Thy1::ChR2 transgenic mice by blue light illumination. Baseline (light-off), 10-Hz and randomized illumination were shown in this video. As compared to baseline, both 10-Hz and randomized protocols provided similar and robust bradykinesia.

FULL METHODS

Animal materials. Male adult Wistar rats entered the study at ~ 8 week-old and 250-350 g. They received behavioral and electrophysiological evaluations and served as both normal and parkinsonian models. For optogenetics experiments, we used male adult Thy1::ChR2-EYFP line 18 transgenic mice (catalog 007612; The Jackson Laboratory), which expresses channelrhodopsin-2 in cortical neuron layer V (13) and has been validated as an ideal animal model for selective stimulation of cortico-subthalamic axons (12, 13). Mice entered the study at ~ 5 week-old and weights heavier than 20 g. The animals were housed in a vivarium with controlled 12-hour dark-light cycles. All procedures were approved by the Institutional Animal Care and Use Committee.

NMDAR and CaT modulators. We used NMDAR blockers with different subunit specificities. (D)-AP5 (2 mM, Tocris) is a non-selective NMDAR blocker. (R)-CPP (200 μM, Tocris) is a selective NMDAR antagonist targeting on GluN2A subunit. RO 25-6891 (1 mM, Tocris) and PPDA (500 μM, Tocris) inhibit GluN2B/D subunit selectively. To inhibit CaTs, we selected $NiCl_2$ (6 mM, Sigma-Aldrich) and mibefradil (500 μM, Tocris). PPDA was dissolved in Dimethyl sulfoxide (DMSO) to 50 mM first and then diluted with saline to make a final concentration of 500 μM. All the other drugs were dissolved in aCSF. The pH of all solutions was adjusted to 7.4.

Generating PD rat model. 6-hydroxydopamine (6-OHDA, Sigma-Aldrich) lesioned hemiparkinsonian rats were used in all the PD experiments in this study. Each Wistar rat was pretreated with desipramine hydrochloride (25 mg/kg, i.p., Sigma-Aldrich) 30 minutes before the 6-OHDA exposure to protect noradrenergic neurons. The rats were anesthetized with chloral hydrate (280-350 mg/kg, i.p., Sigma-Aldrich) and mounted to the stereotactic frame (Kopf Instruments) with a hole drilled on the skull. Brain-lesioning cannula (30-gauge, Braintree Scientific) was slowly inserted into unilateral medial

forebrain bundle (AP -2.8 mm, L 2.0 mm, D 8.0 mm from the bregma point) and left in place for 5 minutes. 8 μg of 6-OHDA (dissolved in 4 μl of normal saline with 0.01% ascorbic acid and protected from light, Sigma-Aldrich) was slowly infused (0.5 μl/min for 8 minutes) and left in place for another 10 minutes. The wound was closed by 4/0 nylon monofilament. 7-10 days after surgery, the 6-OHDA lesioned rats received apomorphine test (0.05mg/kg s.c.). Only rats with robust unilateral rotations (more than 25 turns in 5 minutes) were taken as valid PD models for further experiments.

Implantation of stimulating/recording electrodes and micro-infusion cannula. In valid 6-OHDA or normal control rats, we implanted microwire deep electrodes for single-unit and LFP recordings as well as applying hyperpolarizing currents. Epidural screw electrodes were also implanted for cortical LFPs. A bundle of 6 insulated tungsten electrodes (diameter 0.002 inch, California Fine Wire Company) on a 10-pin connector (Omnetics Connector Corporation) was inserted into the STN (AP -3.8 mm, L 2.4 mm, D 7.5 mm) ipsilateral to the 6-OHDA injection side. There were 5 fixation screws on the skull, one on the nasal bone (AP 5.7 mm, L 0 mm), two on both sides of the premotor cortex (AP 2.7 mm, L ±2.0 mm) and two on the cerebellum (AP -12 mm, L ±2 mm). Nasal screw was wired to the connector as ground electrode. Cortical and cerebellar ones ipsilateral to the deep electrodes were used for epidural and reference electrodes, respectively. Tungsten electrodes were inserted with simultaneous single-unit recordings to identify the characteristic firings of STN. LFPs were recorded in the surface electrodes to ensure stable epidural contacts. A duplex of non-metalic micro-infusion cannula and stimulating electrode (C315G/PK/SP-MS303, PlasticsOne) was also inserted into the same STN coordinates, with 30-degree tilt in the AP plan and 0.1 mm withdrawn to avoid direct contact to the electrodes. The implants were fixed with bone cement, and the wound was closed with 4/0 nylon monofilament. Further experiments were not performed until the body weight and animal behaviors returning to the baseline, which typically took 5-7 days.

Implantation of fiber optic cannula. In order to manipulate the cortico-subthalamic activation and simultaneously observe the behavioral changes in awake animals, fiber optic cannula (CFMC12L05, Thorlabs) was inserted into unilateral STN of Thy1::ChR2 transgenic mice (12, 13). Each mouse was anesthetized with continuous isoflurane infusion via nose piece and mounted to the stereotactic frame with skull exposed. The cannula was implant into STN (AP -1.9 mm, L 1.7 mm, D 4.2 mm) and fixed with bone cement. The rest of surgical procedures were similar to those in rats.

Behavioral tests and analysis. We used open-field test to evaluate the free-moving locomotor behavior in 6-OHDA and control rats. Before the true experiment, each rat was put into a square arena (size: 45 cm x 45 cm) and allowed to move freely for 5 minutes every other day until the behavior was stabilized. To evaluate the behavioral effect of NMDAR and CaT blockers, each drug or aCSF control was infused into the cannula with the speed of 0.4 ul/min for 3 minute, and another 5 minutes with simultaneous behavioral recording by the video-tracking system (Ethovision 3.0, Noldus, Netherland). For each set of experiment, either aCSF or drug was given randomly in the first run, and the other one in the second run. The two runs were separated by least 1.5 hours to avoid carry-over effect. For those rats receiving constant hyperpolarizing currents instead of pharmacological manipulations in STN, we recorded the locomotor behavior for 5 minutes with simultaneous current injection. These rats also received sham stimulation as a self-controlled condition, which was randomly assigned in the first or second run of the experiments. For those rats receiving simultaneous application of drugs and hyperpolarizing currents, they received an additional run of experiment following the drug-infusion protocol with simultaneous current injection during the 5-minute recording in this run. To quantify the behavioral profiles, we extracted 3 parameters from the tracking system, including moving distance, moving velocity and rearing score to represent motility (10-12). Additionally, we chose rotational bias and head tilting bias to represent asymmetric movements (12, 13). The rotational bias was defined by the number of turns rotated toward the side of 6-OHDA lesioning (or fiber optic implant) subtracted by the turns in the

opposite direction, and counted manually on-site. Head tilting bias was defined by the number of head tilts ($>15^0$ deviation from the midline) toward the side of 6-OHDA lesioning subtracted by the number of contralateral deviation, and also counted manually on-site. We also used rotarod test as a forced-moving paradigm. Each rat received 3 runs of 5-minute challenge in each day, with the speed started from 5 round-per-minute (rpm) and ramped up to 60 rpm. Each run was separated for at least 30 minutes. We trained the rats for 3 days, and the behaviors usually became stable at the end of the 2nd day. For those rats received online pharmacological modulations, we used the first run as baseline condition, and performed intracerebral drug infusion (as the protocol above) afterword. We evaluated the modulatory effect by the 2nd and 3rd runs of experiments. For those rats receiving current injection, we injected currents at and only at the 2nd and 3rd runs. Two parameters, including sustained time and maximal velocity, were extracted from the rotarod test.

Optic stimulation and simultaneous behavioral recordings. We activated the cortico-subthalamic axons optogenetically by two different protocols: a frequency-dependent (10 Hz) and frequency-independent (randomized) illumination. A 473 nm diolaser (Crystalaser) was connected to the fiber optic cannula through optic fiber cord. For 10 Hz stimulation, the laser was turned on for 50 ms every 100 ms (duty cycle 50%). For randomized stimulation, the inter-stimulus intervals ranged from 60-125 ms were randomized shuffled (by excel 2013, Microsoft). In this protocol, the stimuli remained 10 pulses per second and lasted 50 ms per pulse, so the stimulation loads were the same as the 10-Hz protocol. In both conditions, we adjusted the averaged light intensity to 4 mW. The mouse was placed into a 40 cm x 20 cm arena equipped with the video tracking system (Smart, Panlab Harvard Apparatus). Behavioral data were recorded after 60 seconds of free movement. In the following 240 seconds of recordings, we separated the data into 5 sections. The baseline (0th~30th second), interstimulus (60th~120th second) and post-stimulus (180th~240th second) sections had no illumination (light-off), intermixed with two illuminating sections (30th~60th and 120th~180th second). Either 10 Hz-fixed or randomized protocol

was randomly assigned into the first illuminating section, followed by the other protocol in the later section. Besides, baseline and two illuminating sections, which we took the full 30 seconds for behavioral analysis, we took the latter half of 1minutes (also 30 seconds) to calculate interstimulus (90th~120th seconds) and post-stimulus (210th~240th seconds) behaviors. The selection is in order to avoid potential transition behaviors when the light was switching off. Behavioral parameters were the same as those used in rats.

In vivo single-unit recordings. Single-unit firings in STN were recorded in rats implanted with microwire electrodes and micro-infusion cannula. After a 5-minute record of the baseline condition, we slowly infused NMDAR or CaT blockers into STN, with the speed of 0.2 μl/min for 8 minutes. To evaluate the drug effect, single-unit recordings were started again 10 minutes after the completion of drug infusion and lasted for 5 minutes. For those STN receiving constant hyperpolarizing currents, we applied 200 μA of positive currents into STN for 5 minutes with simultaneous behavioral recordings, as well as 5-minute baseline prior to the stimulation. For those recordings require simultaneous application of AP5 and hyperpolarizing currents, we followed the drug-infusion protocols, expect an additional 5-minute recording with simultaneous current application. The electrical signals were filtered (300-3,000 Hz band-pass filter), amplified (20,000x), and digitized (sampling rate: 40,000 Hz) with a microelectrode amplifier (Model 3600, A-M System).

Recordings of cortical and subthalamic local field potentials. The LFPs were recorded simultaneously from epidural and deep electrodes continuously for an hour. The rats were placed into the open-field arena, and remained freely movable during the recording period. To evaluate the effect of NMDAR and CaTs, we recorded the baseline condition for 10 minutes and then infused the drug into STN at the speed of 0.2 μl/min for 8 minutes. For rats receiving constant hyperpolarizing currents, we applied 200 μA of constant hyperpolarizing currents for 2-3 minutes after 10 minutes of baseline recording. For those rats

receiving simultaneous AP5 and hyperpolarizing currents, current injection started at 10 minutes after the completion of drug infusion, and lasted for 5 minutes (**Supplemental Figures 5 and 6**). The electrical signals were filtered (0.3-100 Hz band-pass filter), amplified (2,000x), and digitized (sampling rate: 512 Hz) through a microelectrode amplifier (Model 3600, A-M System). Electric signals from the epidural electrode were taken as cortical LFPs. For STN LFPs, signals from one of the 6 deep electrodes were subtracted from each other one by one. Signals from the pair with best quality were used for STN LFPs.

Analysis of single-unit recordings. Signals recorded for single-unit settings were post-processed with the spike-sorting software (SciWorks 8.0, DataWave Technology) and quality controlled algorithm (12). The spikes were identified by threshold detection, and then sorted under the algorithm of principle component analysis (PCA). We only included the sorted units with signal-to-noise ratio >2 and coefficient of variation (CV) > 0.7. Qualified units underwent burst detection based on the following criteria of interval algorithm: maximal interval to start a burst, 20 ms; minimal interval to end a burst, 20 ms; and minimal number of spikes in a burst, 4. We measured the burst-firing rate and intra-burst profiles, including spike count in each burst (spike number), intra-burst inter-spike interval, and burst duration.

Analysis of local field potentials. The LFP data were post-processed with Matlab 7.4 (MathWorks, Natrick). LFP signals were transformed into frequency domain by power spectrum density (PSD) function (PSD by Welch's method with Hanning windowing, sampling rate at 512 Hz in data block of 2 seconds, giving the resolution of 0.5 Hz and half of the data overlap in each step). Each PSD data point was constructed from a 10-second window and one-second shift for the next data point until the end of data stream. We also performed coherence analysis (12) for synchronization between cortex and STN. The value of coherence is between 0 and 1. One indicates perfect linear relationship between the two signals in the given frequency, and zero means completely lack of linear relationship. The coherence data were constructed with the same windowing fractioning, overlapping and time-shifting methodology as

PSD. Based on the simultaneous behavioral observations, we also subdivided the LFP data into moving or resting states. We only extracted those PSD and coherence data from constant moving/resting states for 30 seconds without transition of states. Peak beta PSD and coherence were calculated in beta frequency range (20-50 Hz) in baseline and conditions manipulated by drug infusion, constant current injection, or both.

Statistics. The statistics were managed with SPSS 13.0 (SPSS) and plotted with Excel 2013 (Microsoft). Non-parametric Wilcoxon Signed Rank Test was used to analyze paired data, including animal behaviors, single-unit recordings and LFP analyses (**Figures 1-4 and Supplemental Figures 2-4**). For those data with 3 or more conditions, we applied one-way ANOVA with post-hoc Bonferroni correction (**Figures 5, 6, Supplemental Figures 5 and 6**). In all statistic methods, P value smaller than 0.05 was considered significant.

Immunohistochemistry. 3-month old adult C57BL/6J mice and 4-month old Wistar rats with or without 6-OHDA lesioning were used for immunohistochemistry study. Mice and rats were anesthetized with isoflurane, followed by overdosed urethane (2 g/kg i.p., Sigma-Aldrich) and transcardially perfused with 4% paraformaldehyde in PBS. The brain was then removed and immersed in the 4% paraformaldehyde overnight, and moved to PBS for 3 days. The brain was sliced coronally in the thickness of 30 μm by vibrotome. The sections were washed with PBS, followed by the suppression in 10% normal donkey serum in 0.1% Triton. The sections were subsequently incubated with respective primary antibodies overnight at 4^0C and then secondary fluorescent antibodies (all from Invitrogen). Primary antibodies included GluN2A (Neuromab, Cat. No. 75-288; 1:100 dilution), GluN2B (Neuromab, 75-097; 1:100 dilution), GluN2D (Bioss, Bs-1072R; 1:100 dilution), MAP2 (Abcam, Ab5392; 1:1000 dilution), CaV3.1 (Alomone Labs, ACC-021; 1:100 dilution), CaV3.2 (Alomone Labs, ACC-025; 1:100 dilution) and CaV3.3 (Alomone Labs, ACC-009; 1:100 dilution). Images were taken using confocal laser

scanning microscope (Leica TSC SP2 two photon microscope).

Verification of the implants and 6-OHDA lesions. The locations of deep electrodes were first achieved by the unique firing patterns in STN during implantations. Post-mortem verification was also performed in the brain slices in hematoxylin or Nissl stain. For PD models, the effect of 6-OHDA lesioning was verified by the rotational behaviors in apomorphine test (more than 25 turns in 5 minutes). Tyrosine hydroxylase immunohistochemistry was also used to verify the unilateral loss of dopaminergic neurons in behaviorally confirmed parkinsonian rats (**Supplemental Figure 1**). We only collected data from those animals with correct electrophysiological, behavioral, and histological verifications.

Study approval. The study was approved by Institutional Animal Care and Use Committee (IACUC) of National Taiwan University College of Medicine and College of Public Health